

# Decellularized periosteum promotes guided bone regeneration via manipulation of macrophage polarization

Jiayang Li<sup>1</sup>, Dongming He<sup>2</sup>, Longwei Hu<sup>2</sup>, Siyi Li<sup>2</sup>, Chenping Zhang<sup>2</sup>, Xuelai Yin<sup>2</sup>, and Zhen Zhang<sup>2</sup>

<sup>1</sup>Shanghai Stomatological Hospital

<sup>2</sup>Shanghai 9th Peoples Hospital Affiliated to Shanghai Jiaotong University School of Medicine

February 27, 2023

## Abstract

Periosteum has shown potential as an effective barrier membrane for guided bone regeneration (GBR). However, if recognized as a “foreign body”, insertion of a barrier membrane in GBR treatment will inevitably alter the local immune microenvironment and subsequently influence bone regeneration. The aim of this investigation was to fabricate decellularized periosteum (DP) and investigate its immunomodulatory properties in GBR. DP was successfully fabricated from periosteum from the mini-pig cranium. In vitro experiments indicated that the DP scaffold modulated macrophage polarization toward a pro-regenerative M2 phenotype, which in turn facilitated migration and osteogenic differentiation of bone marrow-derived mesenchymal stem cells. A rat GBR model with a cranial critical-size defect was established, and our in vivo experiment confirmed the beneficial effects of DP on the local immune microenvironment and bone regeneration. Collectively, the findings of this study indicate that the prepared DP possesses immunomodulatory properties and represents a promising barrier membrane for GBR procedures.

## 1 Introduction

Guided bone regeneration (GBR) is a therapeutical strategy widely applied to promote new bone regeneration mainly in the maxillofacial region, especially in cases of periodontal and peri-implant bone defects [1]. As an important step in GBR procedures, a barrier membrane is inserted between the soft tissue defect and the bone defect to prevent ingrowth of competing epithelial and connective tissue [1, 2]. This creates a segregated space for slow-migrating progenitor cells and/or stem cells with osteogenic potential to colonize the defect site and ultimately achieve bone regeneration. Given the key role that the barrier membrane plays in GBR procedures, researchers have continued pursuing novel strategies to develop superior GBR membranes.

Periosteum is a thin vascularized connective tissue that covers the external surface of bone (with the exception of articular bone) and plays a key role in bone regeneration [3, 4]. Periosteum is known to be a niche of progenitor cells and local growth factors, as well as to serve as a natural scaffold for recruitment of cells and biological factors [5, 6]. Additionally, this tissue shows prominent smart material properties, such as direction- and flow rate-dependent permeability [3, 7, 8]. Based on the great potential of periosteum in bone tissue engineering applications, several attempts have been made to apply tissue engineering methods to develop an artificial periosteum that mimics native periosteum in structure and function [9, 10]. To date, however, no tissue engineering strategy has been able to recreate the unique three-dimensional (3D) microenvironment that fully recapitulates the periosteum-specific extracellular matrix (ECM) properties.

In recent years, in the fields of tissue engineering and regenerative medicine, tissue-derived ECM has become an increasingly popular biomaterial source [11-13]. It has been shown that the decellularization process efficiently removes antigenic cellular components while retaining the natural 3D ultrastructure complete with

the native ECM composition. Studies have demonstrated the feasibility of preparing decellularized tissue ECM scaffolds and applied them in the repair of multiple types of tissues and organs with varying degrees of success [14-16]. Although tissue-derived ECM scaffolds are generally used for the repair of non-homologous anatomic sites, site-specific homologous tissue scaffolds have been shown to be more effective than non-site-specific tissue scaffolds in remodeling constructive tissue. Therefore, we speculated that decellularized periosteum, which provides the native ECM derived from periosteum, holds great potential as a GBR membrane. However, the related research is relatively scarce.

Based on the convergence of osteoimmunology and immunomodulation, osteoimmunomodulation has been proposed to be an essential ability of biomaterials for regulating bone regeneration [17, 18]. A fundamental principle underlying this concept is that biomaterials have immunomodulatory properties that are important for generating an osteoimmune environment that facilitates bone regeneration. With more detailed investigations of the interaction between host tissues and biomaterials, the immune response is considered a necessary element in membrane-mediated GBR procedures. Due to its “foreign body” nature, the barrier membrane will inevitably alter the local immune microenvironment and thereby influence the dynamics of bone regeneration [19-21]. Therefore, research efforts to develop improved barrier membranes must consider the osteoimmunomodulatory properties of the membrane material.

In the present study, cranial periosteum of mini-pig was harvested to fabricate decellularized periosteum (DP), which was then characterized. *In vitro*, we investigated the effect of DP on the inflammatory reaction and polarization of macrophages as well as its effect on osteogenesis. *In vivo*, we examined the effectiveness of DP in GBR in rat cranium critical defect model. Collectively, the findings of this study indicate that the DP possesses osteoimmunomodulatory properties and represents a promising membrane for GBR procedures.

## 2 Materials and Methods

The animal experiment protocols were approved by the Animal Experiment Ethics Committee of Shanghai Ninth People’s Hospital affiliated to Shanghai Jiaotong University, China. The studies were designed according to the guidelines of the Animal Research: Reporting of *In Vivo* Experiments (ARRIVE).

### 2.1 Fabrication of DP

The cranium periosteum of mini-pigs was harvested using the following procedure. Briefly, 12-month-old minipigs were anesthetized by intraperitoneal injection of Zoletil (50 mg/kg, Virbac, France). Then the skin and the overlying fascia of the cranium were cut to expose the periosteum. Then the intact periosteum was carefully stripped from the bone surface using a periosteal detacher. The harvested natural periosteum (NP) was prepared for further evaluation or the decellularization process.

The decellularization process for the preparation of DP involved physical, chemical, and enzymatic methods. First a freeze-thaw process (-80, 24 h; 37, 2 h) was repeated three times. Then the obtained samples were treated with 2% Triton X-100 for 12 h followed by 0.5% sodium dodecyl sulfate (SDS) solution for 4 h and 100 U/ml DNase I for 12 h, after which it was soaked in ultrapure water for 3 days to remove the residual treatment reagents. Finally, the fabricated DP was stored in sterile phosphate-buffered saline (PBS) containing 100 U/ml penicillin and 100 µg/ml streptomycin for preservation.

Collagen scaffolds (COL scaffolds) for use as a control were prepared as previously described [22].

### 2.2 Evaluation of decellularization

#### 2.2.1 Histological and immunofluorescent evaluation

For confirmation of decellularization, DP samples were fixed in 4% paraformaldehyde for 24 h and embedded in paraffin. After dehydration and paraffin embedding, the DP samples were cut into 5-µm-thick sections for histological examination using hematoxylin and eosin (H&E) staining. The stained sections were visualized and photographed on an optical microscope (Leica, DM3000, Germany). Residual nuclei within the DP were observed by DAPI staining viewed on an Olympus BX53 microscope (Olympus, Japan).

## 2.2.2 Quantification of DNA, glycosaminoglycan (GAG) and collagen content

The DNA content in DP samples was determined using a Genomic DNA Extraction Kit (Takara, China) following the manufacturer’s instructions. The GAG content in DP samples was evaluated using a DMMB Colorimetry Kit (GenMed, USA). A hydroxyproline assay kit (Abcam, USA) was utilized to quantify the collagen content of DP samples according to the manufacturer’s instructions.

## 2.3 Characterization of DP

The surface morphology of DP scaffolds was analyzed by scanning electron microscopy (SEM; Model: JSM-6700F, JEOL, Japan) and atomic force microscopy (AFM; Model: Multimode & Dimension 3100, Varian, USA). Additionally, the scaffolds were stained with Picrosirius Red (Solarbio, China) and viewed under a polarizing microscopy (Leica, Germany) for observation of the collagen structure. DP samples were also histologically examined using Masson trichrome staining and safranin-O/fast green staining. Immunohistochemical analysis was performed using antibody against type I collagen (dilution: 1:200, Abcam, USA). The surface hydrophilicity was evaluated by measuring the water contact angle with a contact angle goniometer (Dataphysics OCA 35, Germany) using the sessile drop method. The mechanical properties of the DP scaffolds were tested using a universal testing machine (Model: AG-IC 50KN, SHIMADZU, Japan). Dumbbell-shaped samples measuring 4 mm × 50 mm were prepared for mechanical testing, and the cross-head speed was set at 15 mm/min with a load capacity of 50 N. The yield stress, failure strain, and modulus data were obtained.

## 2.4 *In vitro* experiments

### 2.4.1 Cell culture

RAW264.7 cells (murine macrophage cell line) were purchased from the Typical Culture Preservation Commission Cell Bank, Chinese Academy of Sciences (Shanghai, China), and cultured in Dulbecco’s Modified Eagle’s Medium (DMEM, Sigma-Aldrich, USA) containing 10% fetal bovine serum (FBS, Hyclone, USA) at 37 in a humidified incubator with 5% CO<sub>2</sub>. Rat bone marrow-derived mesenchymal stem cells (rBMSCs) were isolated, cultured, and identified utilizing a well-established technique as previously described [22, 23].

The COL and DP scaffolds were placed individually in 96-well plates, and cells were seeded over the scaffolds at a density of 2x10<sup>4</sup> cells/mL. Cells seeded on plates without scaffolds served as controls. Cell proliferation was quantified using the Cell Counting Kit-8 (CCK-8; Sigma, USA) on days 1, 3, and 5 after seeding.

### 2.4.2 Evaluation of the effects of DP scaffolds on macrophage polarization

Cells seeding on different scaffolds were harvested after 3 days, and the impact of DP on macrophage polarization was evaluated by flow cytometry (BD Accuri C6, USA) using antibodies against CD86 (1:50 dilution, BioLegend, USA) and CD206 (1:400, BioLegend, USA) along with Dylight 488-anti-mouse secondary antibodies. The relative levels of inducible nitric oxide synthase (iNOS) and arginase 1 (Arg-1) gene mRNA transcripts relative to the control glyceraldehyde-3-phosphate dehydrogenase (GAPDH) mRNA in the different groups of RAW264.7 cells were quantified by qRT-PCR. The primers sequences used for qRT-PCR are presented in Table 1. For enzyme-linked immunosorbent assay (ELISA) evaluation, the supernatants of RAW264.7 cultures were collected. The concentrations of the cytokines interleukin (IL)-10 and TNF- $\alpha$  in the supernatant samples were quantified using ELISA kits (Dakewe Bioengineering, China) according to the manufacturer’s instructions.

For RNA-sequencing analysis, total RNA was extracted from the tissue samples using TRIzol reagent (Invitrogen, USA), according to the manufacturer’s instructions. cDNA libraries were then constructed for pooled RNA samples using the VAHTSTM Total RNA-Seq (H/M/R) Library Prep Kit (VAHTSTM, China). Differentially expressed genes (DEGs) were identified using TopHat and Cufflinks, and their expression levels were determined by the fragments per kilobase of transcript per million mapped reads method. The DESeq algorithm was used to screen DEGs between groups. The biological functions of the DEGs were then investigated by Gene Ontology (GO) enrichment analysis (<http://www.geneontology.org/>).

### 2.4.3 Evaluation of the effects of polarized macrophages on the proliferation, migration, and differentiation of rBMSCs

To analyze the impact of macrophage polarization on the proliferation, migration, and differentiation of BMSCs, supernatant samples were collected from wells containing macrophages seeded on scaffolds after 3 days of culture to prepare conditioned medium (CM). BMSCs were cultured in 96-well plates and then treated with a mixture of DMEM and CM at a ratio of 1:1. After 1 and 3 days in culture, the CCK-8 assay was performed to evaluate the proliferation of BMSCs.

Wound scratch assays and Transwell assays were performed to evaluate the effects of polarized macrophages on the migration of BMSCs. In the wound scratch assay, BMSCs were seeded in six-well plates with basal medium, once they reached 90–100% confluency, a scratch with the head of 200- $\mu$ L pipette tip (Axygen, USA) was made through the cell layer. Then, serum-free CM was added, and the cells were further incubated for 12 h and 24 h. Cell migration was observed under a microscope (Olympus, Japan), and the healing area was calculated using ImageJ software (NIH, USA). Boyden chambers were used for the Transwell assay. BMSCs were plated in the upper chamber with basal medium, and RAW264.7 cells were seeded on different materials in the lower chambers. After culture for 24 h, the penetrating cells were fixed with 4% paraformaldehyde, stained with crystal violet solution, and counted under an optical microscope (Olympus, Japan).

Alizarin Red staining (ARS) was conducted to evaluate calcium nodule deposition by BMSCs cultured in CM with osteogenic components for 21 days. The rinsed BMSCs were fixed in 4% paraformaldehyde and stained by exposure to 2% ARS solution at room temperature for 20 min. The stained calcium deposits were dissolved by application of 10% cetylpyridinium chloride (Sigma-Aldrich, USA) for 15 min, and dye release was quantified by spectrophotometry at 562 nm (Thermo Fisher Scientific, USA).

The mRNA expression levels of bone morphogenetic protein-2 (BMP2) and runt-related transcription factor 2 (RUNX2) in BMSCs cultured with CM for 3 days were measured using qRT-PCR. The relevant primers sequences are presented in Table 1.

## 2.5 *In vivo* experiments

### 2.5.1 Rat model of cranial defect

Sprague–Dawley rats (male, weighing 280–320 g) were kept in a specific pathogen-free facility with a controlled temperature of  $22\pm 2^\circ\text{C}$ , humidity of  $55\pm 5\%$ , a light/dark cycle of 12/12 h, and free access to water and food. To create the critical-sized defect models, the rats were anesthetized with isoflurane gas, and a skin incision was made to expose the cranium. Then 5-mm-diameter defects were created bilaterally. Then the defects were covered with COL membrane, DP, or left empty (blank control group), and the wound was subsequently closed. All rats were housed and fed routinely until being euthanized at the designated time points.

### 2.5.2 Micro-computed tomography ( $\mu$ -CT) analysis

Cranial samples harvested at 8 weeks post-surgery were fixed in 4% paraformaldehyde. The fixed samples were scanned using  $\mu$ -CT system (Scanco Medical, Bassersdorf, Switzerland) with 70 kV voltage, 114 mA electric current, and 700-ms integration time. The obtained images were analyzed with the software of the  $\mu$ -CT 80 system for 3D construction. Cylinders with 5 mm diameter and 1 mm height were chosen as the volume of interest (VOI). Bone mineral density (BMD) and bone volume/tissue volume (BV/TV) were calculated for quantitative analysis of bone regeneration within each VOI.

### 2.5.3 Histological evaluation

Immediately after  $\mu$ -CT analysis, samples were decalcified and embedded in paraffin. Sections were prepared and subjected to Masson's trichrome staining. The sections were observed under a stereoscopic microscope (Eclipse E600, Nikon, Tokyo, Japan), and the proportion of newly regenerated bone was evaluated using Image-Pro Plus software (Media Cybernetics).

## 2.5.4 Immunohistochemical staining

At 1 week post-surgery, collected tissues were prepared into 10- $\mu$ m-thick sections and stained using primary antibodies targeting the macrophage pan marker CD68 (ab125212, Abcam, USA), M1 phenotype marker iNOS (ab15323, Abcam, USA), and M2 phenotype marker CD206 (ab64693, Abcam, USA). Briefly, dewaxed sections were incubated with primary antibodies overnight and then incubated with secondary antibody for 30 min. The DAB kit (Proteintech, USA) was used to detect immunoreactions, and stained sections were viewed under an optical microscope (Leica DMI 6000B Microsystems, Germany). The proportion of positive cells was calculated under 40 $\times$  magnification.

## 2.6 Statistical analysis

All quantitative data are expressed as mean  $\pm$  standard deviation (SD) values derived from independent experiments with at least triplicate samples. GraphPad Prism v.9.0 software (La Jolla, CA, USA) was employed for data analysis using one-way analysis of variance (ANOVA) with Tukey's post-hoc test. P values  $<0.05$  were considered statistically significant.

## 3 Results

### 3.1 Effectiveness of the decellularization procedure

Macroscopic images of NP and DP are shown in Figure 1A. HE staining of both sample types showed a double-layered (fibrous layer and cambium layer) structure consistent with NP as well as well-organized collagen fibers, but cell nuclei were absent from both layers of DP. Within DP, collagen fibers were still arranged in an orderly manner similar to that in NP (Figure 1B). DAPI staining also confirmed that almost no cellular components or nuclear material could be observed in DP (Figure 1C). The DNA quantification analysis indicated that the amount of DNA in NP was  $526.2 \pm 44.68$  ng/mg, while that in DP was  $38.2 \pm 12.39$  ng/mg (Figure 1D). The quantification of collagen content showed no significant difference between NP and DP ( $115.76 \pm 11.26$  and  $103.20 \pm 13.26$   $\mu$ g/mg dry weight for NP and DP, respectively,  $P > 0.05$ ; Figure 1E). The DMMB results indicated a significant decrease in GAG content in DP ( $1.87 \pm 0.07$   $\mu$ g/mg dry weight) compared with NP ( $3.99 \pm 0.07$   $\mu$ g/mg dry weight,  $P < 0.05$ ; Figure 1F). In addition, only examination of DP and not NP showed no visible bands of DNA detected by agarose gel electrophoresis. In summary, these results indicate the effectiveness of the decellularization procedure for removal of cellular components from periosteum.

### 3.2 Physical and mechanical properties of DP

The surface topographies of collagen, NP, and DP scaffolds were visualized by SEM and AFM (Figure 2A&B). As shown in the SEM images, NP had a relatively smooth surface, while COL and DP displayed uneven and porous surfaces with abundant collagen fibers randomly arranged in a network pattern. Masson trichrome staining revealed the collagen fiber structure in each group (Figure 2C). The structure and distribution of collagen did not differ significantly between DP and NP. Picrosirius red examination also showed that the arrangement and structure of collagen in DP was similar to that in NP (Figure 2D). Immunohistochemical staining of collagen I demonstrated the arrangement of type I collagen in each group (Figure 2E), and Safranin O staining showed the presence of identifiable GAGs in DP scaffolds after decellularization (Figure 2F). The surface hydrophilicity of each scaffold material was analyzed by water contact angle measurement as shown in Figure 2G. Both the NP and DP scaffolds showed good hydrophilicity. Analysis of the mechanical properties of each scaffold type showed no significant difference in yield stress among the groups, but that the DP scaffolds exhibited a moderate elastic modulus (Figure 2H).

### 3.3 Effect of DP on macrophage polarization *in vitro*

CCK-8 analysis results showed that both BMSCs and RAW264.7 cells cultured on each scaffold material maintained similar proliferation activities, with no significant differences found among the groups (Figure 3A&B). Flow cytometric evaluation indicated upregulated expression of the M2-macrophage marker CD206 as well as downregulated expression of the M1-macrophage marker CD86 among RAW264.7 cells in the DP

group (Figure 3C). qRT-PCR results further confirmed that the expression of the M2 macrophage-related gene *ARG-1* was significantly higher, while that of the M1 macrophage-related gene *iNOS* was much lower in the DP group than in other two groups (Figure 3D). Additionally, similar trends in the secretion levels of cytokines IL-10 and TNF- $\alpha$  among the groups were confirmed by ELISA evaluation (Figure 3E).

The transcriptomes of RAW264.7 cells cultured on COL and DP scaffolds were further analyzed. Transcription of 3092 genes in these cells was altered after their culture on DP ( $|\log_2\text{fold change}| > 1$ , false discovery rate [FDR]  $< 0.05$ ), of which 1405 genes were upregulated and 1687 were downregulated (Figure 3F&G). GO enrichment analysis showed that most of the over-expressed genes were associated with regulation of the inflammatory response, antigen processing and presentation, cytokine activity, the major histocompatibility complex (MHC) protein complex, as well as regulation of angiogenesis and vasculature development (Figure 3H). Kyoto Encyclopedia of Genes and Genomes (KEGG) analysis showed that the over-expressed pathways were associated with inflammatory modulation, including the p53 signaling pathway, NF-kappa B signaling pathway, and IL-17 signaling pathway (Figure 3I).

### 3.4 Effect of DP-induced macrophage polarization on BMSC migration and differentiation in vitro

The effects of macrophages cultured on DP on the proliferation, migration, and differentiation of BMSCs were further evaluated. CCK-8 analysis indicated no significant differences in cell proliferation activity among the different groups (Figure 4A). Both wound scratch and Transwell assays showed that BMSC migration was significantly promoted by macrophages seeded on DP scaffolds in comparison to the different control conditions (Figure 4B-E). Additionally, we observed that the CM from macrophages cultured on DP facilitated the osteogenic differentiation of BMSCs, as confirmed by ARS staining as well as changes in the mRNA expression levels of *Runx2* and *BMP2*. The obtained data indicate that CM from macrophages exposed to DP promoted the migration and osteogenic differentiation of BMSCs.

### 3.5 Effectiveness of DP scaffold in a GBR model in vivo

A 5-mm-diameter critical-size defect was established in a rat cranium for our in vivo GBR model. No inflammation or infection was observed at the defect sites in the different groups during the experimental period. Micro-CT was applied to evaluate bone regeneration within the defects in each group. Representative 3D reconstructed images are displayed in Figure 5A. For the blank control group, very little bone formation was found in the defect, whereas newly formed bone tissue was evident in defects treated with COL or DP in a centripetal manner with regenerated bone stretching from the margins toward the center. Quantitative analysis of the micro-CT findings is presented in Figure 5B&C. By week 8, the BMD of newly formed tissues in the control group remained as low as  $282.2 \pm 16.17$  mg HA  $\text{ccm}^{-1}$ . In contrast, the BMD measurements were  $529.3 \pm 22.67$  mg HA  $\text{ccm}^{-1}$  and  $508.1 \pm 14.96$  mg HA  $\text{ccm}^{-1}$  for the COL and DP groups, respectively, and the differences compared with the control group were statistically significant difference ( $P = 0.0266$ ,  $n = 3$ ). For the ratio of bone volume to total volume (BV/TV), similar trends were observed. Bone regeneration was further evaluated histologically with Masson trichrome staining (Figure 5D). In the control group, the defect areas showed poor repair with mainly blue-stained fibrous connective tissues present. In contrast, in the DP group, the defect was filled with woven bone (blue stained) and cortical-like lamella bone (red stained), and a more mature arrangement of collagen also was observed. Quantitative analysis indicated the new bone percentage in the DP group ( $49.1\% \pm 7.69\%$ ) was significantly higher than that in the control group ( $12.2\% \pm 3.94\%$ ;  $P < 0.01$ ) and that in the COL group ( $31.5\% \pm 3.45\%$ ;  $P < 0.05$ ; Figure 5E). These results indicate that DP promoted significantly more bone regeneration within the rat cranial defect GBR model.

To evaluate the osteoimmunomodulatory properties of DP in the early period of GBR, immunohistochemical staining for CD68 (pan marker of in situ macrophages), iNOS (M1 marker), and CD206 (M2 marker) was performed (Figure 5F). Semi-quantitative analysis of the staining results indicated that a greater percentage of CD206+ M2 macrophages ( $64.4\% \pm 7.64\%$ ;  $P < 0.05$ ) was found in the DP group at week 1 compared with the other groups, whereas the number of iNOS+ M1 macrophages in the DP group was relatively low ( $33.6\% \pm 2.52\%$ ;  $P < 0.05$ ; Figure 5G). In summary, these results indicate that DP induced polarization of more M2 phenotype macrophages in the early GBR process.

## 4 Discussion

In the present study, DP was successfully fabricated from periosteum harvested from the mini-pig cranium. In vitro experiments indicated that the prepared DP induced macrophage polarization to the pro-regenerative M2 phenotype, which subsequently facilitated the migration and differentiation of BMSCs to promote osteogenesis. Furthermore, in vivo experiments demonstrated that the prepared DP effectively promoted bone regeneration in a rat GBR model (Scheme 1). These results indicate that DP offers good potential as an osteo-immunomodulatory membrane for use in clinical GBR applications.

The goal of tissue decellularization is to remove as much immunogenic cellular components as possible while preserving the original ultrastructure and composition of the tissue ECM [14, 16, 24]. A variety of techniques can be used to decellularize tissue, including physical agents, chemical agents, and enzymes. Combinations of these techniques have been commonly used to improve the effectiveness of the decellularization process. In the present study, a promising protocol (freeze-thaw processing, Triton-X100, SDS and DNase I) was followed to prepare periosteum that was decellularized to the maximum degree while preserving the intact ECM structure as much as possible. The findings of the present investigation indicate that the prepared DP met the objective standards for decellularization, which generally include: (1) lack of visible nuclear material in tissue sections stained with DAPI or HE; (2) total quantified DNA concentration of less than 50 ng per mg dry tissue weight; and (3) DNA fragment length smaller than 200 bp. Overall, the results in this study demonstrated that the decellularization protocol applied was effective at removing cells from the periosteum tissue [15, 25].

The ideal decellularization procedure should minimize disruption of the ultrastructure and composition of ECM, which is composed of macromolecular fibers, of which type I collagen is one of the most vital structural proteins [16, 26]. Our SEM analysis indicated that the prepared DP retained an irregular fibrous surface architecture similar to the NP architecture, and the collagen integrity remained intact. Quantitative analysis of collagen content showed no significant difference between DP and NP, while relatively lower GAG loss was observed in DP mainly due to its high sensitivity to the decellularization SDS solutions. GAGs also represent an important ECM component and are thought to play a determinant role in the preservation of biological growth factors in decellularized tissues. This finding was consistent with other similar studies [15, 25]. The mechanical stress parameters were almost equivalent between DP and NP, also indicating that the collagen content and alignment were not obviously affected by the decellularization process. Furthermore, due to the increase in porosity with decellularization, the scaffold obtains better hygroscopicity, and the reduced elasticity modulus makes the membrane easier to apply in a bone defect. Overall, the prepared DP retained most of the defining composition and structure of NP.

Grafting of barrier membranes in GBR is known to result in a change in the local immune microenvironment, thereby influencing the subsequent bone regeneration. Immunity plays a key role not only in determining biocompatibility but also in modulating the activities of tissue-resident cells, hence influencing tissue regeneration outcomes. The fields of regenerative medicine and biomaterials science recently have focused on the importance of modulating the host immune response and have noted that rapid resolution of the inflammatory process is essential for tissue regeneration to occur [17, 20]. Ideally, a GBR membrane should synergistically promote both immune and progenitor cells to contribute to successful bone regeneration and avoid stimulation of a detrimental inflammatory response leading to a failure implantation [19, 21, 27]. Therefore, in the present study, we concentrated on the immune microenvironment generated by DP. Our results confirm that the DP scaffold induced macrophage polarization to the M2 phenotype, which effectively promoted the osteogenic differentiation of BMSCs and further bone regeneration.

The immune microenvironment generated by scaffold biomaterials can vary according to the different properties of the biomaterials, including their topological cues, chemistry, porosity, bioactive ion release, etc. [28-31]. Previous studies have reported that ECM derived from diverse source tissues can alter the phenotype of macrophages. For example, when grafted in cranial defects, ECM hydrogel from porcine periosteum was able to induce polarization of macrophages into the M2 phenotype [32]. Additionally, ECM of porcine small intestinal submucosa was shown to regulate a sequential M1-M2 macrophage transition to promote

angiogenesis and osteogenesis both in vitro and in vivo [33]. However, porcine bone-derived ECM particles were reported to induce more M1 phenotype in periodontal defects [34]. In the present study, DP generated a relatively favorable immune microenvironment that supported bone regeneration, and we proposed that this is mainly due to the preservation of the natural ECM structure and composition. The retained original 3D periosteum structure along with biochemical cues including collagen, GAGs, glycoproteins, fibronectin and different growth factors, making this natural biomaterial more biocompetent than single-component collagen membranes.

## 5 Conclusion

In this study, DP derived from mini-pig cranium was successfully fabricated. The present study then focused on the understanding of the modulatory effects of DP in GBR by investigating the involvement of macrophages in this process. The results indicate that DP scaffolds can modulate macrophage polarization to a pro-healing M2 phenotype. Additionally, macrophages polarized by the DP scaffolds supported BMSC migration and differentiation in vitro. Even more importantly, DP adequately improved the proportion of pro-healing macrophages as well as the area of bone regeneration in a rat cranium critical defect GBR model. Overall, our findings indicate that the DP can play an active role in GBR via its immunomodulatory effects rather than its function as a traditional barrier.

### Data Availability Statement:

The data are available from the corresponding author on reasonable request.

## References

- [1] M. Retzepi, N. Donos, Guided Bone Regeneration: biological principle and therapeutic applications, *Clinical oral implants research*, 21 (2010) 567-576.
- [2] R. Dimitriou, G.I. Mataliotakis, G.M. Calori, P.V. Giannoudis, The role of barrier membranes for guided bone regeneration and restoration of large bone defects: current experimental and clinical evidence, *BMC medicine*, 10 (2012) 81.
- [3] Z. Lin, A. Fateh, D.M. Salem, G. Intini, Periosteum: biology and applications in craniofacial bone regeneration, *Journal of dental research*, 93 (2014) 109-116.
- [4] C. Colnot, X. Zhang, M.L. Knothe Tate, Current insights on the regenerative potential of the periosteum: molecular, cellular, and endogenous engineering approaches, *Journal of orthopaedic research : official publication of the Orthopaedic Research Society*, 30 (2012) 1869-1878.
- [5] B.G. Matthews, S. Novak, F.V. Sbrana, J.L. Funnell, Y. Cao, E.J. Buckels, D. Grcevic, I. Kalajzic, Heterogeneity of murine periosteum progenitors involved in fracture healing, *eLife*, 10 (2021).
- [6] S.R. Moore, C. Heu, N.Y. Yu, R.M. Whan, U.R. Knothe, S. Milz, M.L. Knothe Tate, Translating Periosteum's Regenerative Power: Insights From Quantitative Analysis of Tissue Genesis With a Periosteum Substitute Implant, *Stem cells translational medicine*, 5 (2016) 1739-1749.
- [7] H. Chang, M.L. Knothe Tate, Concise review: the periosteum: tapping into a reservoir of clinically useful progenitor cells, *Stem cells translational medicine*, 1 (2012) 480-491.
- [8] N. Li, J. Song, G. Zhu, X. Li, L. Liu, X. Shi, Y. Wang, Periosteum tissue engineering-a review, *Biomaterials science*, 4 (2016) 1554-1561.
- [9] Y. Zhu, B. Dai, X. Li, W. Liu, J. Wang, J. Xu, S. Xu, X. He, S. Zhang, Q. Li, L. Qin, T. Ngai, Periosteum-Inspired Membranes Integrated with Bioactive Magnesium Oxychloride Ceramic Nanoneedles for Guided Bone Regeneration, *ACS applied materials & interfaces*, 14 (2022) 39830-39842.
- [10] Y. Kang, L. Ren, Y. Yang, Engineering vascularized bone grafts by integrating a biomimetic periosteum and beta-TCP scaffold, *ACS applied materials & interfaces*, 6 (2014) 9622-9633.

- [11] X. Nie, D.A. Wang, Decellularized orthopaedic tissue-engineered grafts: biomaterial scaffolds synthesised by therapeutic cells, *Biomaterials science*, 6 (2018) 2798-2811.
- [12] D.A. Taylor, L.C. Sampaio, Z. Ferdous, A.S. Gobin, L.J. Taite, Decellularized matrices in regenerative medicine, *Acta biomaterialia*, 74 (2018) 74-89.
- [13] K.E. Benders, P.R. van Weeren, S.F. Badylak, D.B. Saris, W.J. Dhert, J. Malda, Extracellular matrix scaffolds for cartilage and bone regeneration, *Trends in biotechnology*, 31 (2013) 169-176.
- [14] G.I. Barbulescu, F.M. Bojin, V.L. Ordodi, I.D. Goje, A.S. Barbulescu, V. Paunescu, Decellularized Extracellular Matrix Scaffolds for Cardiovascular Tissue Engineering: Current Techniques and Challenges, *International journal of molecular sciences*, 23 (2022).
- [15] K. Chen, X. Lin, Q. Zhang, J. Ni, J. Li, J. Xiao, Y. Wang, Y. Ye, L. Chen, K. Jin, L. Chen, Decellularized periosteum as a potential biologic scaffold for bone tissue engineering, *Acta biomaterialia*, 19 (2015) 46-55.
- [16] A.D. McInnes, M.A.J. Moser, X. Chen, Preparation and Use of Decellularized Extracellular Matrix for Tissue Engineering, *Journal of functional biomaterials*, 13 (2022).
- [17] K. Okamoto, T. Nakashima, M. Shinohara, T. Negishi-Koga, N. Komatsu, A. Terashima, S. Sawa, T. Nitta, H. Takayanagi, Osteoimmunology: The Conceptual Framework Unifying the Immune and Skeletal Systems, *Physiological reviews*, 97 (2017) 1295-1349.
- [18] H.Y. Dar, Z. Azam, R. Anupam, R.K. Mondal, R.K. Srivastava, Osteoimmunology: The Nexus between bone and immune system, *Front Biosci (Landmark Ed)*, 23 (2018) 464-492.
- [19] S. Jin, R. Yang, C. Chu, C. Hu, Q. Zou, Y. Li, Y. Zuo, Y. Man, J. Li, Topological structure of electrospun membrane regulates immune response, angiogenesis and bone regeneration, *Acta biomaterialia*, 129 (2021) 148-158.
- [20] K. Wang, W.D. Hou, X. Wang, C. Han, I. Vuletic, N. Su, W.X. Zhang, Q.S. Ren, L. Chen, Y. Luo, Overcoming foreign-body reaction through nanotopography: Biocompatibility and immunoisolation properties of a nanofibrous membrane, *Biomaterials*, 102 (2016) 249-258.
- [21] Z. Chen, L. Chen, R. Liu, Y. Lin, S. Chen, S. Lu, Z. Lin, Z. Chen, C. Wu, Y. Xiao, The osteoimmunomodulatory property of a barrier collagen membrane and its manipulation via coating nanometer-sized bioactive glass to improve guided bone regeneration, *Biomaterials science*, 6 (2018) 1007-1019.
- [22] Y. Xuan, L. Li, M. Ma, J. Cao, Z. Zhang, Hierarchical Intrafibrillar Mineralized Collagen Membrane Promotes Guided Bone Regeneration and Regulates M2 Macrophage Polarization, *Frontiers in bioengineering and biotechnology*, 9 (2021) 781268.
- [23] Z. Zhang, Z. Li, C. Zhang, J. Liu, Y. Bai, S. Li, C. Zhang, Biomimetic intrafibrillar mineralized collagen promotes bone regeneration via activation of the Wnt signaling pathway, *International journal of nanomedicine*, 13 (2018) 7503-7516.
- [24] R. Junka, X. Zhou, W. Wang, X. Yu, Albumin-Coated Polycaprolactone (PCL)-Decellularized Extracellular Matrix (dECM) Scaffold for Bone Regeneration, *ACS applied bio materials*, (2022).
- [25] J. He, Z. Li, T. Yu, W. Wang, M. Tao, Y. Ma, S. Wang, J. Fan, X. Tian, X. Wang, Y. Lin, Q. Ao, Preparation and evaluation of acellular sheep periosteum for guided bone regeneration, *Journal of biomedical materials research. Part A*, 108 (2020) 19-29.
- [26] G.K. Chalikias, D.N. Tziakas, Biomarkers of the extracellular matrix and of collagen fragments, *Clinica chimica acta; international journal of clinical chemistry*, 443 (2015) 39-47.
- [27] C. Chu, J. Deng, X. Sun, Y. Qu, Y. Man, Collagen Membrane and Immune Response in Guided Bone Regeneration: Recent Progress and Perspectives, *Tissue engineering. Part B, Reviews*, 23 (2017) 421-435.

- [28] C. Wu, Z. Chen, D. Yi, J. Chang, Y. Xiao, Multidirectional effects of Sr-, Mg-, and Si-containing bioceramic coatings with high bonding strength on inflammation, osteoclastogenesis, and osteogenesis, *ACS applied materials & interfaces*, 6 (2014) 4264-4276.
- [29] Z. Chen, A. Bachhuka, F. Wei, X. Wang, G. Liu, K. Vasilev, Y. Xiao, Nanotopography-based strategy for the precise manipulation of osteoimmunomodulation in bone regeneration, *Nanoscale*, 9 (2017) 18129-18152.
- [30] X. Dong, P. Wu, L. Yan, K. Liu, W. Wei, Q. Cheng, X. Liang, Y. Chen, H. Dai, Oriented nanofibrous P(MMD-co-LA)/Deferoxamine nerve scaffold facilitates peripheral nerve regeneration by regulating macrophage phenotype and revascularization, *Biomaterials*, 280 (2022) 121288.
- [31] X. Dong, S. Liu, Y. Yang, S. Gao, W. Li, J. Cao, Y. Wan, Z. Huang, G. Fan, Q. Chen, H. Wang, M. Zhu, D. Kong, Aligned microfiber-induced macrophage polarization to guide schwann-cell-enabled peripheral nerve regeneration, *Biomaterials*, 272 (2021) 120767.
- [32] P. Qiu, M. Li, K. Chen, B. Fang, P. Chen, Z. Tang, X. Lin, S. Fan, Periosteal matrix-derived hydrogel promotes bone repair through an early immune regulation coupled with enhanced angio- and osteogenesis, *Biomaterials*, 227 (2020) 119552.
- [33] L. Yang, J. Zhou, K. Yu, S. Yang, T. Sun, Y. Ji, Z. Xiong, X. Guo, Surface modified small intestinal submucosa membrane manipulates sequential immunomodulation coupled with enhanced angio- and osteogenesis towards ameliorative guided bone regeneration, *Materials science & engineering. C, Materials for biological applications*, 119 (2021) 111641.
- [34] R.X. Wu, X.T. He, J.H. Zhu, Y. Yin, X. Li, X. Liu, F.M. Chen, Modulating macrophage responses to promote tissue regeneration by changing the formulation of bone extracellular matrix from filler particles to gel bioscaffolds, *Materials science & engineering. C, Materials for biological applications*, 101 (2019) 330-340.

**Table 1.** Primer sequences for qRT-PCR

Gene name	Forward (5' – 3')	Reverse (5' – 3')
<i>Gapdh</i>	ATGATTCTACCCACGGCAAG	CTGGAAGATGGTGTATGGGTT
<i>Arg1</i>	CGCCTCAAATCCAGCTGTAAG	GGGCCACAATCCAGTCGTT
<i>iNos</i>	TGGTGAAAGTGGTGTCT	TTCCCTGTCTCAGTAGCA
<i>Runx2</i>	CCGAACTGGTCCGCACCGAC	CTTGAAGGCCACGGGCAGGG
<i>Bmp2</i>	TCAAGCCAAACACAAACAGC	CCACGATCCAGTCATTCCA

## Figure Legends

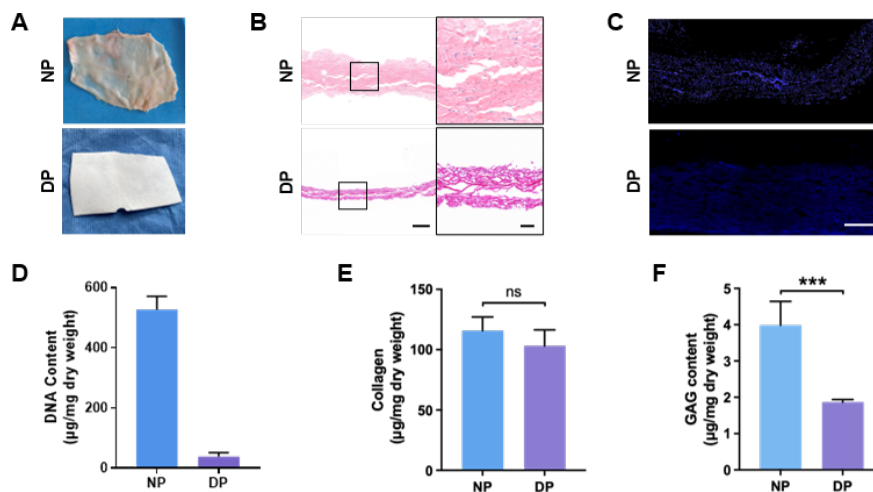


**FIGURE 1** ? Confirmation of cell removal from decellularized periosteum (DP).

(A) Macroscopic images of natural periosteum (NP) and DP. (B) H&E staining of NP and DP. Scale bar, 500  $\mu\text{m}$  and 100  $\mu\text{m}$ . (C) DAPI staining of NP and DP. Scale bar, 100  $\mu\text{m}$ . (D) DNA content quantification. (E) Collagen content quantification. (F) GAG content quantification.

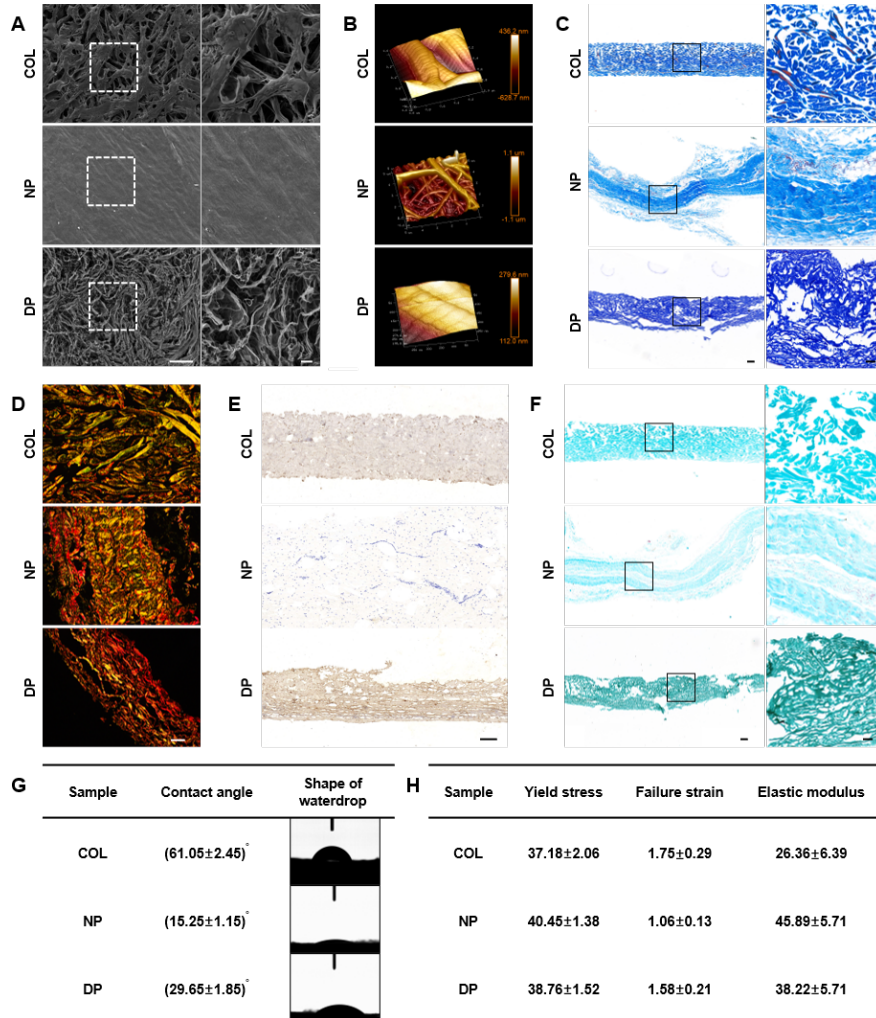


**FIGURE 2** ? Characterization of DP.

(A) Representative SEM images and (B) AFM images showing the surface topographies of collagen, NP, and DP scaffolds. (C) Masson trichrome staining of each scaffold type. (D) Picrosirius red analysis of the collagen fiber structure in each group. (E) Immunohistochemical staining for type I collagen. (F) Safranin-O staining for GAG retention. (G) Water contact angle and waterdrop shape for each scaffold type. (H) Mechanical properties of collagen, NP, and DP scaffolds. (A,C,F) Scale bar, 200  $\mu\text{m}$  and 50  $\mu\text{m}$ . (D,E) Scale bar, 200  $\mu\text{m}$ .

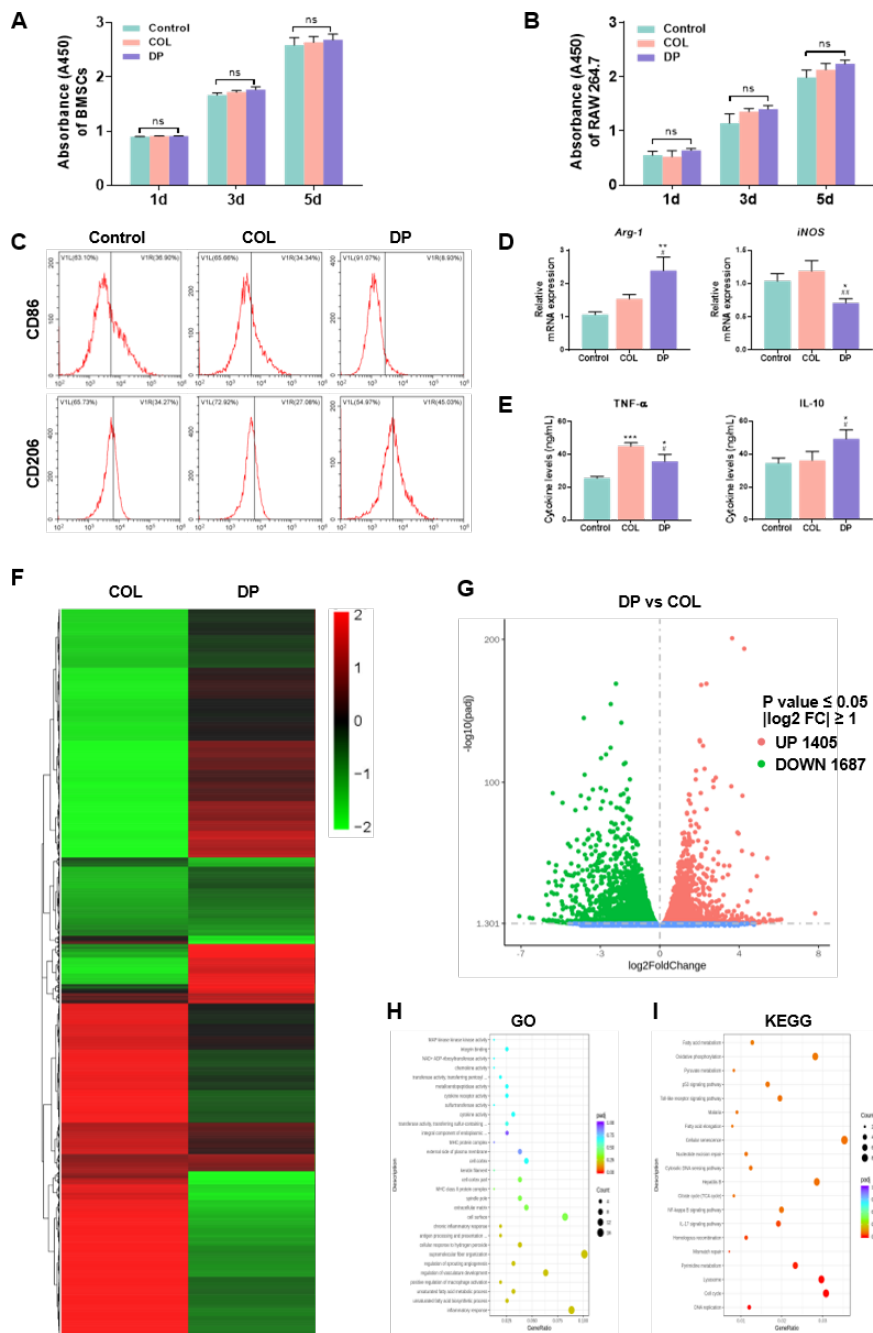


**FIGURE 3 ? DP scaffolds regulate macrophage polarization in vitro.**

(A) Viability of BMSCs seeded on each scaffold type at the indicated time points. (B) Viability of RAW264.7 cells seeded on each scaffold type at the indicated time points. (C) Flow cytometric analysis of macrophage population expressing CD86 (M1 type) and CD206 (M2 type) at 3 days after seeding. (D) mRNA levels of Arg-1 and iNOS in macrophages on the 3<sup>rd</sup> day in culture determined by qRT-PCR. (E) IL-10 and TNF- $\alpha$  levels in the supernatants on the 3<sup>rd</sup> day in culture as detected by ELISA. (F) Heatmap of the transcriptomes of RAW264.7 cells after 3 days in culture on COL and DP scaffolds. (G) Volcano plots of differentially expressed genes (DEGs) between the COL and DP groups. (H) Gene Ontology (GO)

enrichment analysis. (I) Kyoto Encyclopedia of Genes and Genomes (KEGG) analysis.

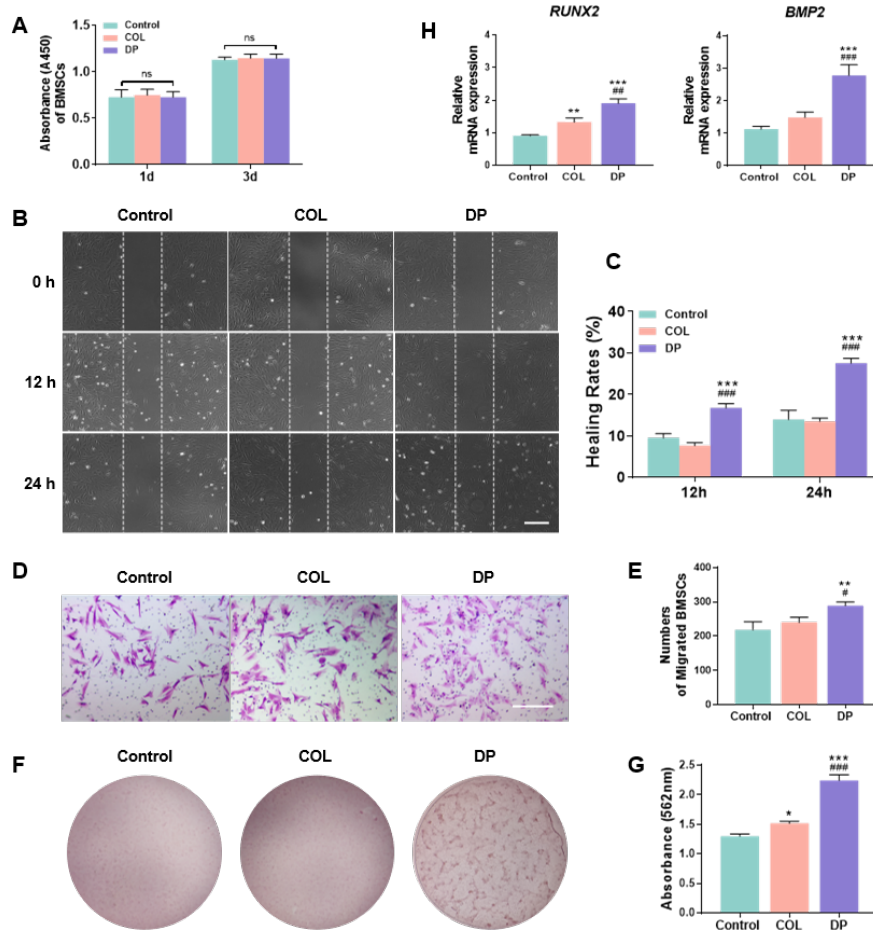


**FIGURE 4** ? Macrophages polarized in response to DP scaffold promote BMSC migration and differentiation in vitro.

The viability of BMSCs after culture in different types of conditioned medium (CM) for 1 and 3 days. (B&C) Representative images and quantitative analysis of BMSC migration after culture in different CM for 1 day. Scale bar, 50  $\mu$ m. (D&E) Transwell-based BMSC migration assays and quantification analysis. Scale bar, 1 mm. (F) ARS staining on the 21<sup>th</sup> day in culture. (G) Quantitative results of ARS staining on the 21<sup>th</sup> day culture. (H) mRNA levels of *Runx2* and *BMP2* in BMSCs after culture in different CM as quantified by qRT-PCR.

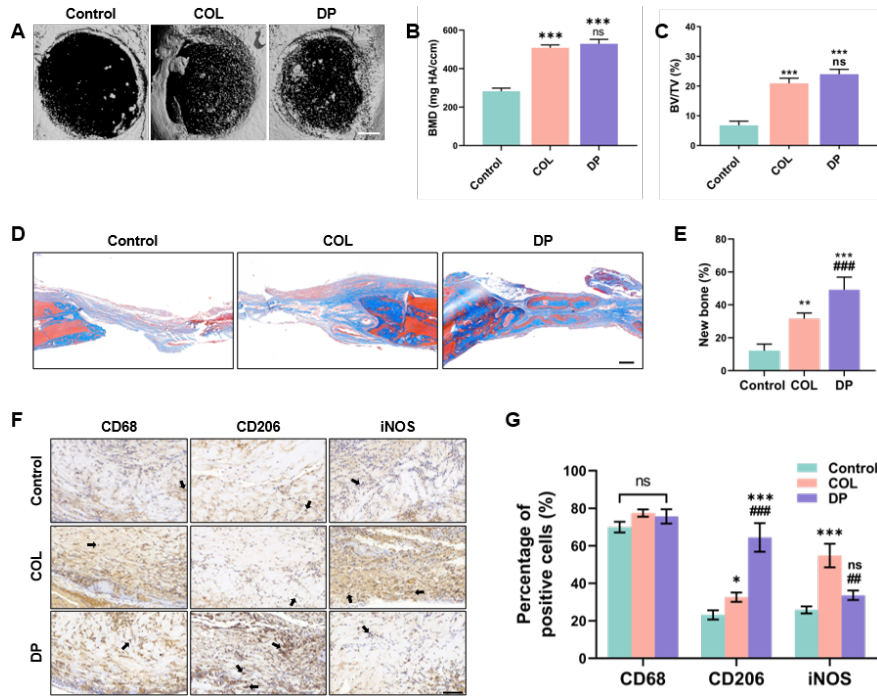
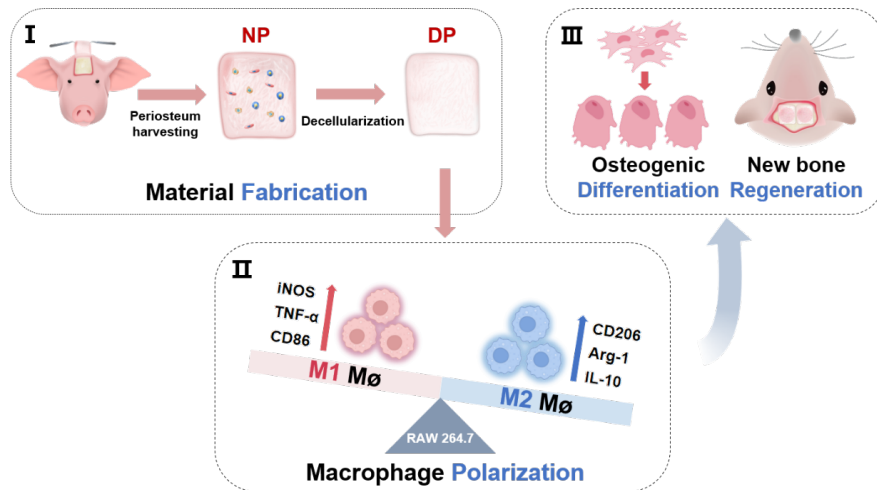


**FIGURE 5 ?** In vivo bone regeneration with a rat critical-sized defect as a guided bone regeneration (GBR) model.

(A) Three-dimensional construction and representative micro-CT images for each scaffold group. Scale bars, 1 mm and 5mm. (B and C) Quantitative results for BMD and BV/TV. (D) Representative images of Masson trichrome staining of samples collected in the 8th week post-surgery. Scale bar, 200  $\mu$ m. (E) Quantitative results for percentage of new bone growth. (F) Immunohistochemical staining for macrophage polarization pan marker CD68, M1 marker iNOS, and M2 marker CD206 in tissue filling the defect tissues. Positively stained cells are indicated by arrows. Scale bar, 100  $\mu$ m. (G) Quantification of positively stained cells.



**Scheme 1 ?** Schematic illustration of bone regeneration in the GBR model promoted by DP via regulation

of macrophage polarization towards the M2 phenotype.